ELSEVIER

Polymer 43 (2002) 4503–4514

polymer

www.elsevier.com/locate/polymer

Chemical and mechanical properties of vinyl-ester/ABS blends

D. Stevanovic[a,*], A. Lowe[b], S. Kalyanasundaram[b], P.-Y.B. Jar[c], V. Otieno-Alego[d]

[a]*Design Office—Mount Stromlo Observatory, Research School of Astronomy and Astrophysics, The Australian National University, Cotter Road, Weston, Canberra, ACT 2611, Australia*

[b]*Department of Engineering, Faculty of Engineering and Information Technology, The Australian National University, Canberra, ACT 0200, Australia*

[c]*Department of Mechanical Engineering, University of Alberta, Edmonton, Alta, Canada T6G 2G8*

[d]*Raman Microscopy Unit, University of Canberra, Canberra, ACT 2601, Australia*

Abstract

Various experimental techniques and finite element modelling (FEM) were employed to assess mechanical and chemical properties of vinyl-ester (VE)/poly(acrylonitrile–butadiene–styrene) (ABS) blends with different ABS particle content. The blends were to be used as a toughening agent for interlayer toughened VE/glass composite material. Firstly, the materials' fracture toughness and tensile properties were examined, the results showing excellent toughening potential of the blends as well as a non-linear trend for fracture toughness as a function of ABS weight content. The tensile testing of the blends served to define the yield point of the materials and to obtain their stress–strain curves, which were then used as input into finite element analysis models. The mechanical testing results suggested that a chemical reaction may have occurred between the constituents of the blends. Based on the Raman spectroscopy results and mechanical testing data, 7% of ABS was believed to be the critical ABS content where significant changes in the materials' chemical composition and consequently in mechanical properties occurred. Finally, FEM was undertaken to further verify the existence of this sudden variation in material's properties.

Keywords: Polymer blends; Rubber toughening; Fracture toughness

1. Introduction

In the last two decades, various attempts have been made to improve the fracture and impact resistance of fibre reinforced composite materials. Chai [1,2] found that the composite's toughness can be directly correlated to the matrix toughness. Therefore, matrix toughening has been a natural first step towards toughness improvement of the composite. However, good resin fracture toughness does not always result in a significant improvement of the composite's toughness. This has been attributed to constraint effects, produced by small interfiber distances that are usually insufficient for full plastic zone development in front of the crack tip [3]. An approach, called interleaving, interlaminar or interlayer toughening [4,5], has been introduced, that shows promising results in the improvement of composite fracture resistance. This method involves the introduction of discrete layers of a neat thermoplastic [4,5] or thermosetting [6] material embedded between the composite plies. This approach recognizes the major importance of the interlayer thickness, which has to allow full formation of the plastic zone in front of a crack tip whilst maximizing the fracture energy absorption. This observation was also made by Chai [1,2,7,8], working on adhesively bonded joints and serve as a good model for the interlayer toughened composites. The major drawback of this approach was a weight penalty associated with the thermoplastic interleaf film, together with the problems of poor adhesion between the film and the composite plies [4,5].

A similar approach involved the use of rubber and/or thermoplastic particles for interlayer toughening, by blending the particles into the composite's matrix during laminate fabrication procedure [3,9–12]. However, with this material system, the toughened interlayer thickness could not be controlled directly, as it could with the homogeneous layers. Nevertheless, this approach has the advantage of avoiding the weight penalty, while maintaining a good delamination resistance and compressive strength after impact. The development of this material resulted in a full commercial product, Torayaca pre-preg T800H/3900-2, that was used in the primary structures of a commercial airliner (Boeing 777). The only shortcoming of these materials has been poor mode I delamination resistance, due to the interfacial crack growth [12]. The latest improvement in particulate interlayered composite materials has been the use of ionomers applied along the toughened layer/composite

* Corresponding author. Tel.: +61-2-61250213; fax: +61-2-61250233.
E-mail address: dejan@mso.anu.edu.au (D. Stevanovic).

0032-3861/01/$ - see front matter
PII: S0032-3861(02)00283-5

lamina interface. Their approach significantly improved the toughness of the interface and the composite [13]. This novel improvement highlighted the importance of good toughened layer—composite bonding and compatibility between the toughening agent (particles) and the composite's matrix when assessing toughness improvement under different loading modes. The use of particles for toughening introduced a new variable which could influence fracture toughness of the composite: particle concentration inside the interlayer. A number of researchers [9–11,14] examined the influence of this variable on fracture toughness. However, the presence of the particles in the layer makes the overall stress distribution extremely complicated. Therefore, the toughening mechanisms in this type of material system are yet to be fully understood.

It is therefore of great importance and interest to understand the relationship between the toughness increase and the chemical/mechanical interaction between constituents of the composite matrix. The understanding also facilitates future experimental study and numerical modelling for development of a successful toughening agent for interlayer toughening of composite materials. As a result, we selected poly(acrylonitrile–butadiene–styrene) (ABS) as a model toughening agent to assess its effect on fracture and tensile properties of glass-fibre-reinforced vinyl-ester (VE) composite. The main variable is ABS weight content in the interlayer region. In addition to the mechanical testing, Raman spectroscopy and finite element modelling (FEM) were used to analyse the chemical and mechanical interactions, respectively, to establish the basic fracture behaviour and toughening mechanisms in the toughened interlayer region of the composite material.

It is therefore obvious that for the production of a successful toughening agent for interlayer toughening of composite materials, a full understanding of the material and its fracture behaviour should be of prime concern. Also, by establishing some basic chemical and mechanical relationships between the material's constituents, before being applied within the composite, an important milestone can be established for any future experimental or numerical modelling study of the material. Accordingly, the main aim of this study was the assessment of fracture and tensile properties of VE/ABS blends with the ABS weight content as the main variable. In order to obtain a full explanation of the experimental results and observed material's behaviour, Raman spectroscopy techniques and finite element analysis were used. This study served to estimate toughening potential of the blends, together with establishing basic fracture behaviour and toughening mechanisms.

2. Materials and preparation

The materials used in this study were Dow Chemicals Derakane 8084 VE resin mixed with ABS particles provided by DENKA Co. of Japan. Four different particle weight concentrations were used: 3.5, 7, 11 and 15%. The ABS powder was dried in a vacuum oven for 5 h at 50 °C and mixed with the resin using a high-speed shear blender (SILVERSON L4RT). A satisfactory mixing procedure was achieved by using three different mixing heads using mixing speeds in the range 7000 and 7500 cycles/min. The blended VE resin was then further mixed with additives which serve to control the speed of the resin solidification process. For this purpose, 1.5% methyl-ethyl-ketone peroxide was used as a 'promoter' (the supplied VE was pre-promoted by the manufacturer with 0.3% of cobalt naphthenate) together with 0.2% of 2,4pentanedione (2,4P) used as a 'retarder' in the chemical reaction. After that, the prepared resin was degassed and poured into prepared aluminium moulds and left for 24 h to cure under atmospheric pressure and room temperature. After an initial room temperature cure in the mould, each plate was post-cured at 90 °C for 4 h to ensure uniform material properties.

Neat resin specimens for mode I fracture testing and tensile testing were machined and prepared from cast plates of modified resins according to the ASTM D5405-91a [15] and ASTM D638M-91a [16] testing standards, respectively. Test specimens were cut using a water-cooled diamond saw and dried in a vacuum oven at 50 °C for 12 h, prior to the testing. Also, some of the specimens were polished to obtain optical micrographs of the particle distribution using a Zeiss Axioscope optical microscope. Polishing was carefully conducted using five different grades of sand paper (from 220 to 1200 grit) and 6 μm diamond paste, which was shown to be sufficient for the purpose of this study.

The ABS tensile specimens were prepared from commercially available ABS plates obtained from the All Plastics Co. of Australia. The material contained approximately the same amount of rubber as the one used for the blends and therefore possessed almost identical mechanical properties.

For the purpose of Raman studies, there is not a specific size requirement for the specimen. The only constraint is that they are physically small enough to fit under the microscope stage. In order to obtain characteristic Raman spectra, small samples of test material taken from the tensile test program were used and cut to approximately 1 cm^2 blocks.

3. Experimental techniques and modelling

3.1. Tensile testing

Uniaxial tensile testing of neat VE, toughened VE and pure ABS plastic was conducted using standard dog-bone specimens according to ASTM D638M-91a [16]. All specimens were machined to have a cross-section at the 'neck' of 2.5 × 3.5 mm (± 0.01 mm) and were tested on an Instron 4505 Universal Testing Machine using strain gauges to measure uniaxial extension of the specimen during the

testing. Data were collected for calculating the Young's modulus, the yield stress and strain, and the failure (break point) stress and strain, for each material.

According to ASTM D638M-91a, the yield point (plasticity onset) is defined as the point where the increase in strain is no longer followed by the subsequent increase in stress (i.e. the maximum stress point in the case of our materials). In this study, it was decided to use the 5% offset (of ε_{max}) yield point as the onset of irreversible deformation, based on observed fracture and yielding behaviour during the test and it will be discussed in the following text. The definition of the yield point is depicted in Fig. 1.

3.2. Mode I fracture toughness testing using SENB specimens

In addition to the tensile testing, mode I fracture toughness of the neat VE and toughened resins was measured using single-edge-notched bend (SENB) specimens according to ASTM D5405-91a [15]. Nominal specimen dimensions were width, $W = 16$ mm and thickness, $t = 8$ mm with a U-notch milled to a depth of 7 mm with a tip radius of 0.5 mm. A natural crack was introduced by tapping a new razor blade placed in the U-notch, to produce a total crack length (a) in the range $0.45 < a/W < 0.55$. Testing was performed using a three-point bend fixture with a span length ($2L$) of 64 mm using a cross-head speed of 10 mm/min.

3.3. Raman spectroscopy

The Raman technique [17,18] is a simple one and involves irradiation of a sample with monochromatic light. The majority of this light is elastically scattered unchanged from the sample, but a small fraction will interact with the sample's vibrational modes and be scattered inelastically (Raman scattering). The variation in wavelength of this Raman scattering will vary with the origin bond in the sample and hence the signal may be collected as a spectrum, and the various peaks that occur can be assigned to specific bonds.

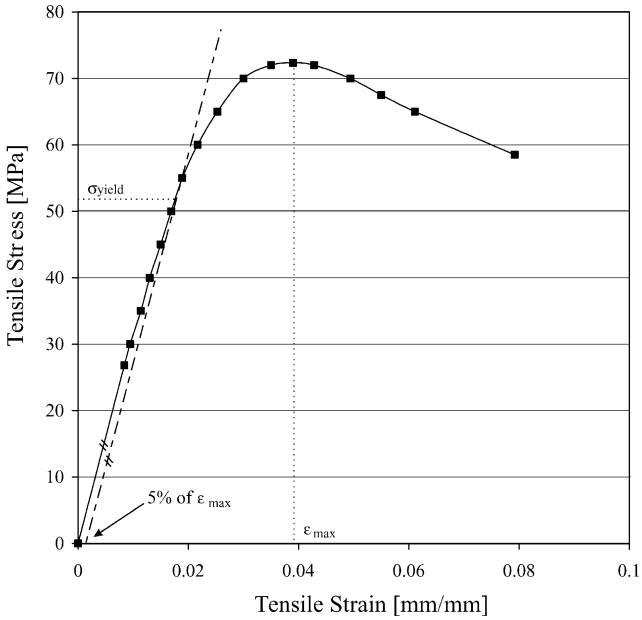

Fig. 1. The typical stress–strain curve obtained from a neat VE specimen with definition of the yield point, being the intersection point of the curve and an offset line drawn from the 5% ε_{max} point and parallel to the elastic part of the curve.

In the field of advanced composite materials, the Raman technique has become extremely important for three reasons. Firstly, like infrared spectroscopy and associated techniques, the Raman technique can provide a spectrum of characteristic bandwidths which can be used to identify the chemical species and bond types present in a material under test. The advantage of the Raman technique over infrared is in the fact that the spectra obtained by the former technique are not masked by the presence of water molecules or hydrolysis products (a big problem with infrared techniques that give strong signals from polar species, such as O–H bonds). The strongest Raman signals originate from symmetrical bonds, such as C–C and C=C. Secondly, the concept of strain mapping has become very useful. This is where a grid or line of spectra is obtained, and so long as an appropriate calibration is available, any shift in characteristic Raman peaks can be attributed to straining of the material, through external or internal stressing. This technique is often used in the detection of interfacial phenomena in composite materials [19–22]. Thirdly, the Raman technique can provide important information on what has now become the most pressing issue in advanced materials research—degradation. Raman analysis of a material both before and after environmental ageing, gives information relating to degradation products and chemical modification, in addition to quantitative data regarding the change in the relative amounts of two or more species/bond types as ageing progresses. In addition, apart from chemical changes invoked by aging processes, this technique can be successfully used for assessing chemical modifications in constituents after blending. Any positional or size variations in characteristic Raman peaks can be directly linked to changes in the material, either through bond stretching, as with the strain mapping technique, or through chemical changes caused by the degradation or during blending process. It is important to note that although the Raman technique has many advantages over other techniques, one major disadvantage is that if water molecules actually need to be detected (quite common during hydrothermal ageing experiments) the Raman signal associated with O–H stretching is quite weak, and often masked by other species. The use of this technique is therefore limited to the detection and quantifying of changes in other chemical species as a result of water addition, i.e. an indirect approach.

An example of this third use is the focus of the current study, where the Raman is used to assist in the identification of any chemical changes that may occur in the VE resin in

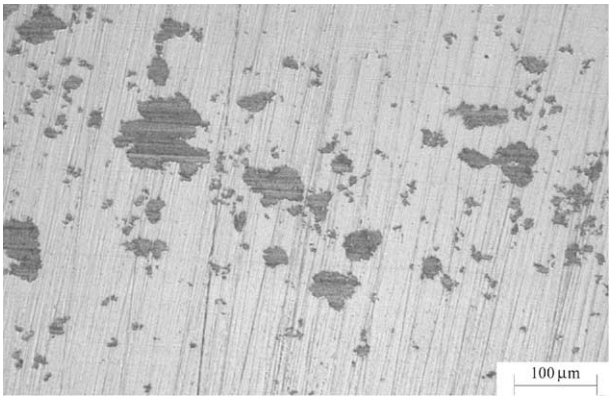

Fig. 2. ABS particle distribution inside a toughened VE—particles are irregular in shape, while size varies from 5 to 150 μm.

the addition of small amounts of ABS. For this purpose, comparative Raman spectra were obtained for neat cured VE, pure ABS plastic and cured VE/ABS blend, prepared by mixing 3.5% of ABS with VE.

3.4. Finite element modelling

In order to give more information on some issues raised by the experimental study, a finite element analysis study was initiated. For this purpose, a small section 200 × 200 μm filled with randomly sized spherical particles, randomly distributed under uniaxial tension loading was modelled. A model of this size was chosen in order to obtain a representative particle distribution, and to maintain the numerical efficiency of the model. FRANC2DL [23] finite element code was employed to solve the corresponding plane stress model made from approximately 7000 second-order isoparametric elements using an elastic–plastic incremental scheme. To obtain the randomness in size and distribution of the particles, an algorithm was developed using a uniform random number generator to produce a particle distribution for an area of given boundaries. More details about the algorithm are given in Ref. [28]. Prior to particle generation, a statistical distribution of ABS particle sizes was devised based on optical micrographs of polished SENB specimens, as shown in Fig. 2.

An attempt to accurately simulate the realistic particle distribution would result in a model with extremely large number of elements due to the existence of numerous particles smaller than 5 μm in diameter. This would result in highly numerically inefficient model without improving the quality of the simulation. Therefore, the main objective of the analysis was to simulate accurate particle concentrations (i.e. bulk properties of the material), rather than exact particle size distributions. Nevertheless, the modelled particle size was random but kept between 10 and 150 μm. Also, the irregular particle shapes visible in Fig. 2 were neglected, under the assumption that the influence of the particle shape is negligible for this study. This assumption was based on experimental results elaborated in Ref. [28]. Material properties used in the analysis were taken from the tensile testing results.

In addition to this model, two further models were developed using regular particle arrays (square and hexagonal) with a uniform particle size of 40 μm in diameter (the average particle size used in the random model). The number of elements used in these two regular array models was approximately 5500. The aim of this was to support results obtained from the random model and to estimate the influence of the particle distribution randomness on the tensile properties.

4. Results and discussion

4.1. Tensile and fracture toughness testing

The main aim of the tensile testing was to establish input parameters for the subsequent numerical analysis and to give a better understanding of the materials' mechanical behaviour before being applied as toughening agents into the fibre composite. Firstly, the neat VE 8084 resin was tested and the results were compared with the material's typical properties obtained from the manufacturer (Dow Chemicals). As expected, the results presented in Table 1

Table 1
Tensile and mode I fracture properties for ABS-modified VE resins (standard deviations are given in parentheses)

ABS (%)	E (MPa)	σ_y (MPa)	σ_{max} (MPa)	ε_{max} (%)	G_{Ic} (J/m^2)	K_{Ic} (MPa $\sqrt{m}$)	r_p (μm)
0 (DC)	3172	–	69–76	–	–	–	–
0	3297(156)	51.2	72.8(0.7)	3.9(0.14)	307(16)	1.1	23
3.5	3043(61)	39.8	57.6(1.5)	2.9(0.2)	737(43)	1.6	86
7	2948(129)	34.2	49.2(1.2)	2.8(0.2)	711(86)	1.5	108
11	2781(38)	31.7	46.5(0.5)	3.5(0.26)	993(25)	1.8	166
15	2585(85)	30.8	41.4(0.8)	3.3(0.27)	1182(18)	1.9	195
100	2540(59)	35.6	35.6(0.6)	1.6(0.12)	1382[a]	2.0[b]	167

0% stands for the neat VE, while 100% stands for the neat ABS; DC stands for Dow chemicals.
[a] Calculated using K_{Ic}.
[b] From Ref. [24].

for the VE 8084 (i.e. 0% of ABS) reflect excellent agreement with the typical properties obtained by Dow Chemicals [26]. The VE specimens failed after passing the maximum stress point at approximately 8% strain without exhibiting any necking. Although specimen necking was absent, significant whitening was observed even before the maximum stress level was reached.

During the testing, all ABS-toughened VE resins failed at the point of maximum stress, which decreased with increasing ABS content, as shown in Fig. 3. Accordingly, it can be noticed that ABS particle addition weakened the unmodified VE, lowering the failure stress.

Although, the tensile curves indicate a possibility of brittle-like failure for all VE/ABS blends, the observations during the test showed significant whitening of the material without necking, possibly caused by substantial micro-cracking and/or yielding of the plastic prior to main failure. Also, as in the case of the neat VE, stress whitening was observed before the maximum stress point. It is known that stress whitening is a proven sign of material plastic deformation [25] suggesting that the onset of plastic deformation for the tested VE/ABS blends and the neat VE occurred prior to the maximum stress point. Therefore, it was necessary to define more precisely the yield point, which is crucial to the proposed FEM analysis. A new set of specimens was tested in order to capture the yielding onset and to establish a consistent definition of the yield point for all materials. Two types of measurements were conducted to relate the onset of the stress whitening to permanent deformation of the material. In the first case, the specimens were loaded up to the stress level where the whitening was initially observed. At that point they were taken out from the test grips and their length was measured with a micrometer and compared with the initial length before testing. The second method utilized the strain measurement capabilities of the Instron testing machine using a strain gauge. After the onset of stress whitening, the test was stopped and after unloading, the strain measurement would be checked for any residual permanent deformation. All measurements were repeated with three specimens. Both measurement approaches produced identical results, supporting the assumption of the yield point existence before the failure. The next step was to provide a consistent definition of the yield point. By careful observation of the deformation during the test, the stress level associated with onset of stress whitening was indicated on the recorded stress–strain curves. After summarizing the test data, it was found that the intersection of the recorded stress–strain curves and the 5% strain offset line defined with high accuracy recorded the onset of stress whitening. Accordingly, the 5% offset yield stress was chosen to represent the yield point for all VE-based materials in this study.

Finally, testing of the neat ABS gave a failure strain of approximately 20%, mainly due to significant necking, as shown by the typical stress–strain response in Fig. 4. The necking reflects the significant presence of shear yielding that occurs in this multiphase polymer [25], which usually results in a stress whitening effect.

A low departure from linearity was observed on the stress–strain curves for all tested plastics, and this was believed to be associated with significant non-linear elastic behaviour due to the presence of rubber particles. The same conclusion can be drawn for neat VE 8084 which has been

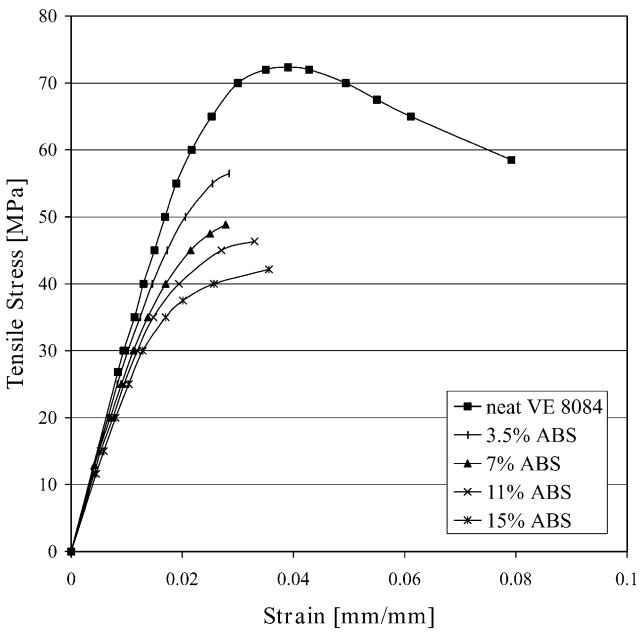

Fig. 3. Stress–strain curves of the neat VE and VE/ABS blends for various percentages of ABS addition—increase in ABS content clearly influenced a drop in the Young's modulus and the maximum and failure stress level of the blends.

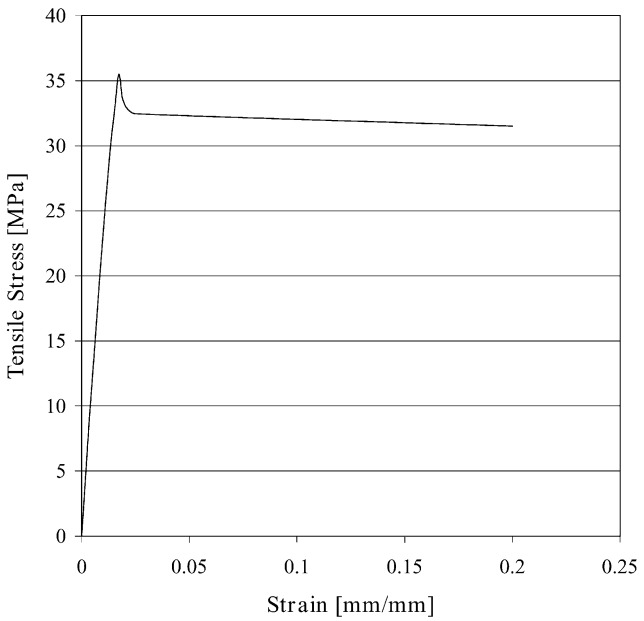

Fig. 4. Stress–strain curve of the neat ABS—after the yield point ABS behaves as an elastic-perfectly plastic material, having the failure strain of approximately 20%.

chemically enhanced by grafting an elastomer (butadiene) onto the backbone of the polymer chain [26]. The reason for this enhancement was to improve fracture toughness.

A summary of the tensile and fracture test results is also presented in Table 1. Clearly, modifying the VE with ABS results in an increase in fracture toughness; a decrease in the Young's modulus and yield strength and subsequent enlargement of the plastic zone developed in front of the crack tip, calculated according to Irwin's plastic zone correction [27]. The variation of mode I fracture toughness with ABS weight content is illustrated in Fig. 5.

An initial increase with 3.5% ABS addition, from 300 to 700 J/m^2 is noted, followed by a plateau region between 3.5 and 7%. Beyond that level of ABS addition, there is a further linear increase in G_{Ic} tending towards a fourfold increase in the fracture toughness at 15% ABS addition, compared to the neat VE 8084. Clearly, the fracture toughness tests revealed the significant toughening potential of the blends. An explanation for the plateau region in the G_{Ic}/ABS% trend and the subsequent increase in toughness might be associated with a chemical reaction between the constituents invoked during mixing and curing procedures. As a consequence, the region on the chart in Fig. 5 around 7% of ABS addition represents a transition in the fracture toughness trend. The possible chemical reaction which may be responsible for such a toughness trend may be the dissolution of butadiene from the ABS into the VE. Since butadiene is present in the unmodified VE in order to improve toughness, it is reasonable to assume that additional amounts of butadiene may cause a further increase in fracture toughness. Also, a saturation level of butadiene addition may exist, leading to the definition of a composition-based saturation point. This can be related to the transitional zone around 7% of ABS weight content, where the change in the fracture toughness trend was noticed. Beyond this level of ABS modification, some additional toughening mechanisms are triggered, resulting in further toughness improvements.

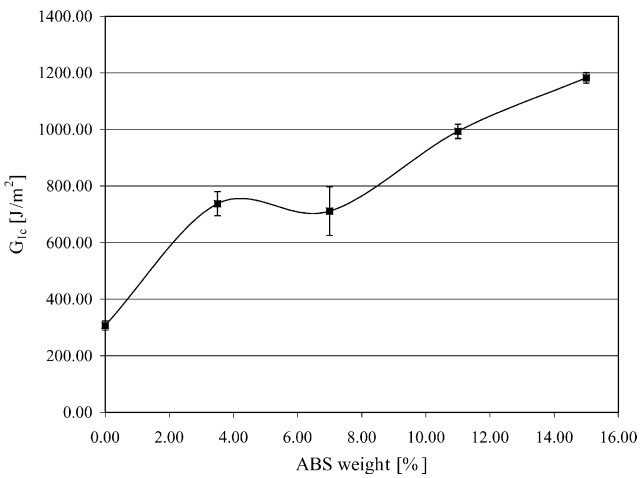

Fig. 5. Mode I fracture toughness as a function of ABS weight content (error bars represent standard deviation)—7% ABS represents a change point in the fracture toughness trend.

SEM fracture surface examination of selected SENB specimens strengthened these assumptions. Fig. 6 depicts typical fracture surfaces from 3.5 to 7% ABS/VE blends.

ABS particles remained visible after the crack propagation, suggesting that they were not influencing crack propagation and eventually resulted in a brittle-like fracture pattern. Some amount of plastic deformation in the VE matrix is obvious, but it is not severe and is probably not solely induced by the particle presence. A similar fracture surface obtained for 7% ABS addition supports this conclusion. Regardless of the twofold increase in particle content, fracture toughness was unchanged, as was the fracture pattern. This leads to the possibility that chemical modification of the VE by the ABS addition could cause a change in the toughening potential of these blends, causing the observed toughness increase. By increasing the ABS content beyond 7%, the fracture surface started to show a significant increase in plastic deformation of the materials, as shown in Fig. 7. Particles are not visible at the fracture

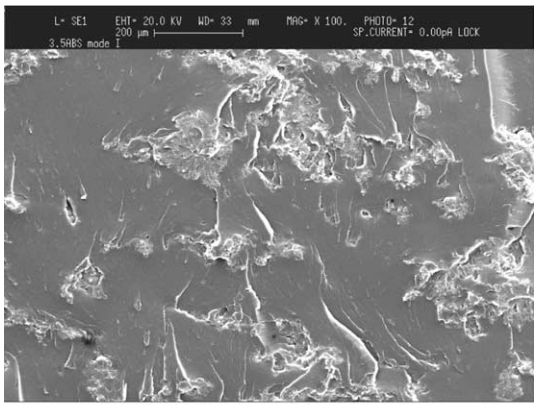

(a) 3.5% ABS

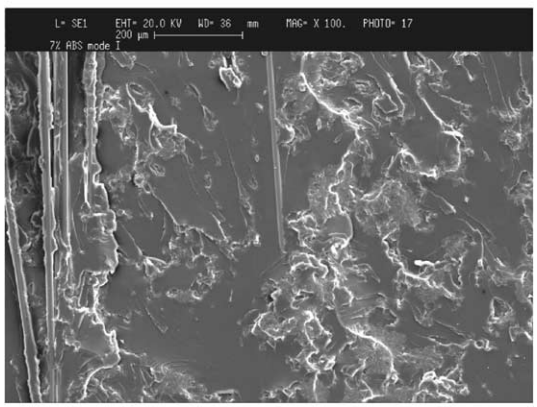

(b) 7% ABS

Fig. 6. SEM images of the typical 3.5 and 7% ABS/VE blend fracture surfaces (crack propagates from bottom to top)—ABS particles are visible together with some amount of plastic deformation, they did not significantly influence crack propagation (crack propagated through the particles).

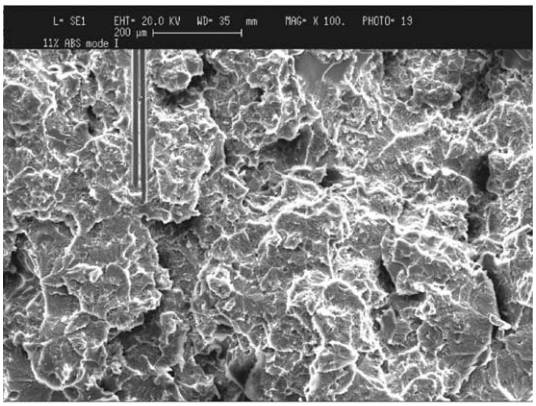

(a) 11% ABS

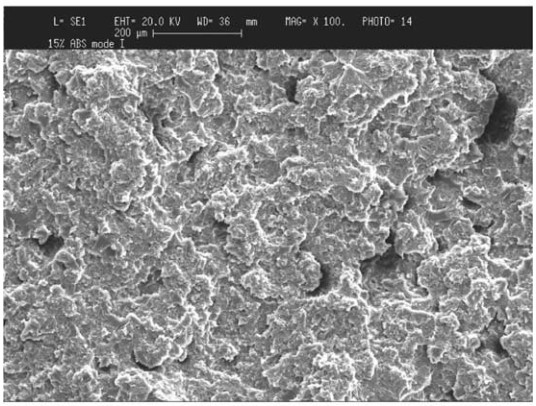

(b) 15% ABS

Fig. 7. SEM images of the typical 11 and 15% ABS/VE blend fracture surfaces (crack propagates from bottom to top)—ABS particles are not visible on the fracture surface which shows signs of severe plastic deformation.

surface due to the extensive whitening and deformation of the material.

Beyond 7% ABS addition, there was a significant change in the fracture pattern. The visible increase in the material's plastic deformation during the crack propagation corresponds well with the increase in measured fracture toughness seen in Fig. 5. It can be assumed that at some level of ABS modification between 7 and 11%, a significant change in the mechanical properties of the blends occurs. This transitional level of ABS content separates materials with different toughening trends and with different governing toughening mechanisms. Therefore, in order to collect more information on possible chemical reactions between the constituents and the materials' composition, Raman spectroscopy techniques were employed.

4.2. Raman spectroscopy

Derakane VE 8084 is a complex material, containing a DGEBA backbone that has been internally modified with a reactive acrylonitrile–butadiene copolymer. The ABS is

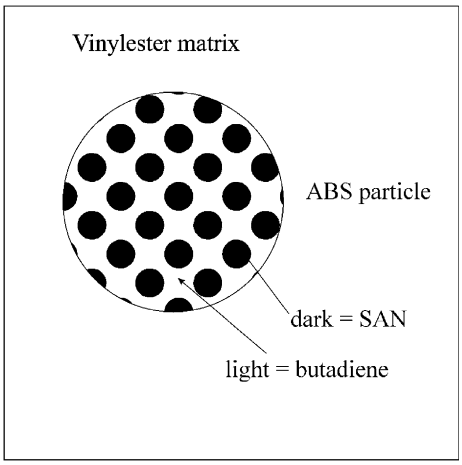

Fig. 8. Schematic showing the phases present in ABS-toughened VE resin (single ABS particle only).

also quite complex, consisting of small regions of styrene acrylonitrile (SAN) embedded within a butadiene-based matrix, giving the combined structure shown schematically in Fig. 8.

The chemical structures of the 8084 backbone, methacrylate ester, SAN and butadiene are as shown in Fig. 9. The VE resin is produced by the reaction of methacrylate monomers with the backbone molecule in the presence of a catalyst, and occurs at room temperature. With reference to Fig. 9, further polymerisation occurs by cleavage of the C=C double bonds. The central R group is a proprietary group consisting of *para*-substituted aromatic rings, acrylonitrile groups and butadiene.

For the purpose of this study, three types of Raman spectra were obtained. Typical spectra from the cured neat untoughened resin (denoted VE), the pure particulate additive (ABS) and the cured complete system with 3.5 wt% ABS addition (VE/ABS blend) are shown in Fig. 10. The assignments of the significant peaks marked 1–15 have been made, and are listed in Table 2.

Clearly, some of the numbered peaks occur in all three spectra, whereas others do not. The areas of the peaks are

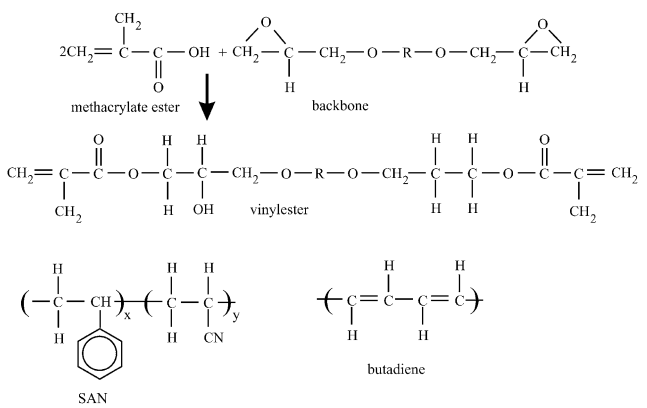

Fig. 9. Chemical formulae for the VE reactants (ester monomer and DGEBA backbone) and the constituents of the rubber particles (SAN and butadiene).

Table 2
Vibrational assignments for the significant Raman bands in the cured VE, ABS particles and their blend

Peak	Wave no. (cm^{-1})	Assignment	Relative areas	
			VE	VE/ABS
1	621 (m)	Ring deformation (aromatic)	1.306	2.791
2	640 (m)	Ring deformation (aromatic)	1	1
3	820 (m)	H_3C-C stretch	6.785	13.46
4	1001 (vs)	Ring breathing (aromatic)	11.547	20.537
5	1032 (s)	CH in-plane bend (aromatic)	2.747	6.021
6	1113 (m)	C–O stretch (ester)	2.214	1.924
7	1156 (w)	CH in-plane bend (aromatic)	0.539	1.687
8	1183 (m)	CH in-plane bend (aromatic)	1.255	4.507
9	1198 (sh)	CH in-plane deformation (alkene)	2.94	8.842
10	1302 (w)	CH_2 twist/rock	1.764	1.845
11	1450 (m)	CH_2 deformation	3.913	3.961
12	1582 (w)	C=C stretch (aromatic)	0.52	0.757
13	1604 (m)	C=C stretch (aromatic)	2.965	4.730
14	1667 (w)	C=C stretch (aliphatic)	0.283	0.723
15	2236 (w)	C≡N stretch (acrylonitrile)	0.171	0.55

Abbreviations: w, weak signal; sh, shoulder signal; m, moderate signal; s, strong signal; vs, very strong signal.

required to assess quantitative information to see how the amount of one species has changed in relation to another. It is important to note that areas of peaks can only be compared *on the same spectrum* and not from one spectrum to another. However, the ratios of one peak to another can be compared across spectra and it is this comparison that makes the Raman technique useful in assessing chemical reactions. In order to make meaningful comparisons, the peak areas need to be referenced to a common peak in each of the spectra of interest, and this peak must be one that remains constant throughout the spectra (i.e. is unaffected by the mixing process). Such a peak occurs at a bandwidth of 640 cm^{-1}. Therefore, to investigate the spectral changes in the material that occur on curing and/or mixing with ABS, the areas of the significant peaks shown in Fig. 10 were normalized relative to the area of the selected internal standard peak at 640 cm^{-1}. This peak can be attributed to *para*-substituted deformation of the benzene rings present in the cured VE backbone. The calculated relative areas for the cured untoughened material and the cured toughened material are also shown in Table 2. Fig. 10 shows that the *para*-substituted groups responsible for the peak at 640 cm^{-1} do not occur in the ABS, hence their omission from Table 2. The information shown in Fig. 10 yields several insights into how the ABS particles and VE interact during curing and/or mixing process. Comparison of spectra shows that on curing of a VE/ABS mixture, much of the contribution from the butadiene in the ABS particles (characterized by the C=C aliphatic stretch at a wavenumber of 1667 cm^{-1}) disappears. There could be several explanations for this, including the breakage of the C=C bond during the curing process due to some reaction. However, the most likely explanation is that on mixing, the butadiene component in the ABS dissolves into the VE matrix, thus resulting in a weaker signal (Raman examination was performed in areas of material known to contain particles). This is borne out by microscopic evidence presented in Ref. [28] that shows partial dissolution of the butadiene matrix occurring at low ABS concentrations.

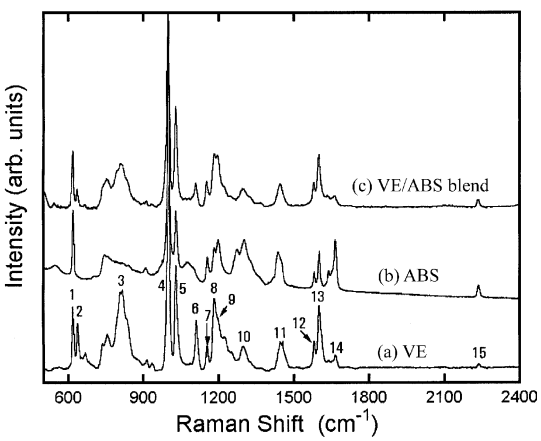

Fig. 10. Raman spectra obtained for (a) cured neat untoughened resin-VE, (b) ABS particles, and (c) VE/ABS blend. The numbers correspond to significant peaks.

4.3. Hypothesis on the composition of the blends

All experimental results presented so far identified the region around 7% ABS addition as a transitional zone in fracture toughness characteristics, possibly induced by the butadiene saturation at this level of ABS. However, at this stage a hypothesis will be made that based on the Raman spectroscopy results that indicated butadiene dissolution from the ABS into VE at low levels of ABS addition (e.g. 3.5% ABS/VE blend), and using the fracture toughness trends seen in Fig. 5, 7% ABS addition represents the butadiene saturation point. A transition in the materials' mechanical properties also occurs at this point. At low levels

of ABS addition, VE is clearly enriched with butadiene and it possesses different properties to the initial VE. Obviously, increased amounts of butadiene improve the fracture toughness of the VE. This was clearly noticed with the 3.5 and 7% ABS blends.

On the other hand, ABS particles, by losing butadiene, become almost pure styrene–acrylonitrile (SAN). Beyond the saturation point, the amount of butadiene in the VE was unchanged, since saturation has been reached, but the renewed presence of butadiene in the particles brought their properties close to the initial ABS. All of this suggests that the particles do not strongly influence fracture toughness values below the saturation point. This conclusion is supported by the similar fracture toughness values at 3.5 and 7% ABS addition levels and is reflected in their fracture surface micrographs illustrated in Fig. 6. It is possible that the toughness values of these VE/ABS blends are higher than that of the neat VE due to chemical modification of the VE, through increased butadiene content. This leads to the conclusion that it is only beyond the saturation point that the complete ABS particles start to influence toughness, possibly by increasing stresses and strains in the surrounding matrix promoting its micro-cracking and yielding. The butadiene migration is presented in Fig. 11.

An important consequence of these observations is that the properties of the matrix beyond the saturation point can be approximated to the bulk properties of the 7% ABS/VE blend while the properties of the particles correspond to the properties of the neat ABS. However, this assumption cannot be fully proved by the existing experimental results, so FEM was employed to support this hypothesis.

4.4. Finite element modelling

After defining the nature and extent of the VE chemical modification by ABS particle addition, FEM was employed to obtain further insights into the existence of a butadiene saturation point and its influence on the materials' mechanical properties. The main purpose of the FEA modelling was to simulate tensile testing of the 15% ABS/VE blend, by employing a model that represents a small rectangular region of matrix $0.2 \times 0.2\ mm^2$ in size filled with randomly distributed spherical particles of random size.

According to the hypothesis on composition of the blends, bulk 7% ABS/VE blend properties were used for the matrix while neat ABS properties were used for the particles. The properties of ABS are assumed to follow an elastic/perfectly plastic stress–strain curve, which corresponds to the experimentally obtained curve illustrated in Fig. 4. ABS particle concentration was equal to the measured particle concentration within the 15% ABS/VE blends. This concentration was found to be 27% of the area, and more details on this measurements will appear in Ref. [28]. In order to prove the assumed particle influence above and below the saturation point, the model was subjected to a uniaxial quasi-static tensile loading and it was expected that it would produce a stress–strain curve that follows the experimentally obtained stress–strain curve for the 15% ABS/VE blend, as depicted in Fig. 3. By fulfilling this expectation, the composition hypothesis used in the models would subsequently proved to be correct.

Fig. 12 depicts the final refinement of the mesh used for the analysis. The mesh is reasonably refined at the matrix/particle interfaces where the highest stresses were expected. A tensile stress was applied at top of the model and gradually increased from 0 to 46 MPa in 2 MPa steps. After each step an average strain was measured along two cross-sections of the model. The latter were chosen to be at $y = 0.195$ and 0.074 mm, measured from the bottom of the model, as illustrated in Fig. 12.

Applied boundary conditions simulated double symmetry (e.g. a quarter of the whole plate was modelled). The results are presented in Fig. 13 in a form of stress–strain curves obtained from the analysis.

It can be noticed that the numerical tensile curves from both cross-sections follow relatively similar trends, which are comparable to the 15% ABS/VE blend stress–strain curve obtained experimentally. The stiffness of the numerical model in the linear-elastic region lies in between two experimental curves, but after exceeding the yield stress of the ABS (36 MPa), rapid straining of the ABS particles occurred, producing curves which followed the experimentally obtained trend of the 15% ABS/VE blend. Differences between the test and modelling clearly exist, but they are acceptable due to the initial simplifications of the model regarding material properties and geometry of the particles.

Although not shown, results obtained from regular array models produced almost identical material responses to those for the random model. Obviously, particle distribution did not have a strong influence on the tensile response of the models. Possibly, a much stronger influence was from the particle concentration, which was identical for all developed models.

The models proved the initial assumption on the existence of 7% ABS as the butadiene saturation point to be correct. Additionally, they directly supported the assumption that at ABS concentrations beyond the saturation point, the particles possess properties similar to those of the neat ABS, while the matrix possesses properties of the saturated VE/ABS blend. The randomness of the model did not have a significant influence on the bulk material properties, but it is reasonable to assume that it can contribute to a more accurate assessment of the stress and strain distribution.

5. Conclusions

The main conclusions of the study are as follows:

(1) Toughening of the Derakane 8084 VE resin with ABS particles was extremely effective, making their blends more

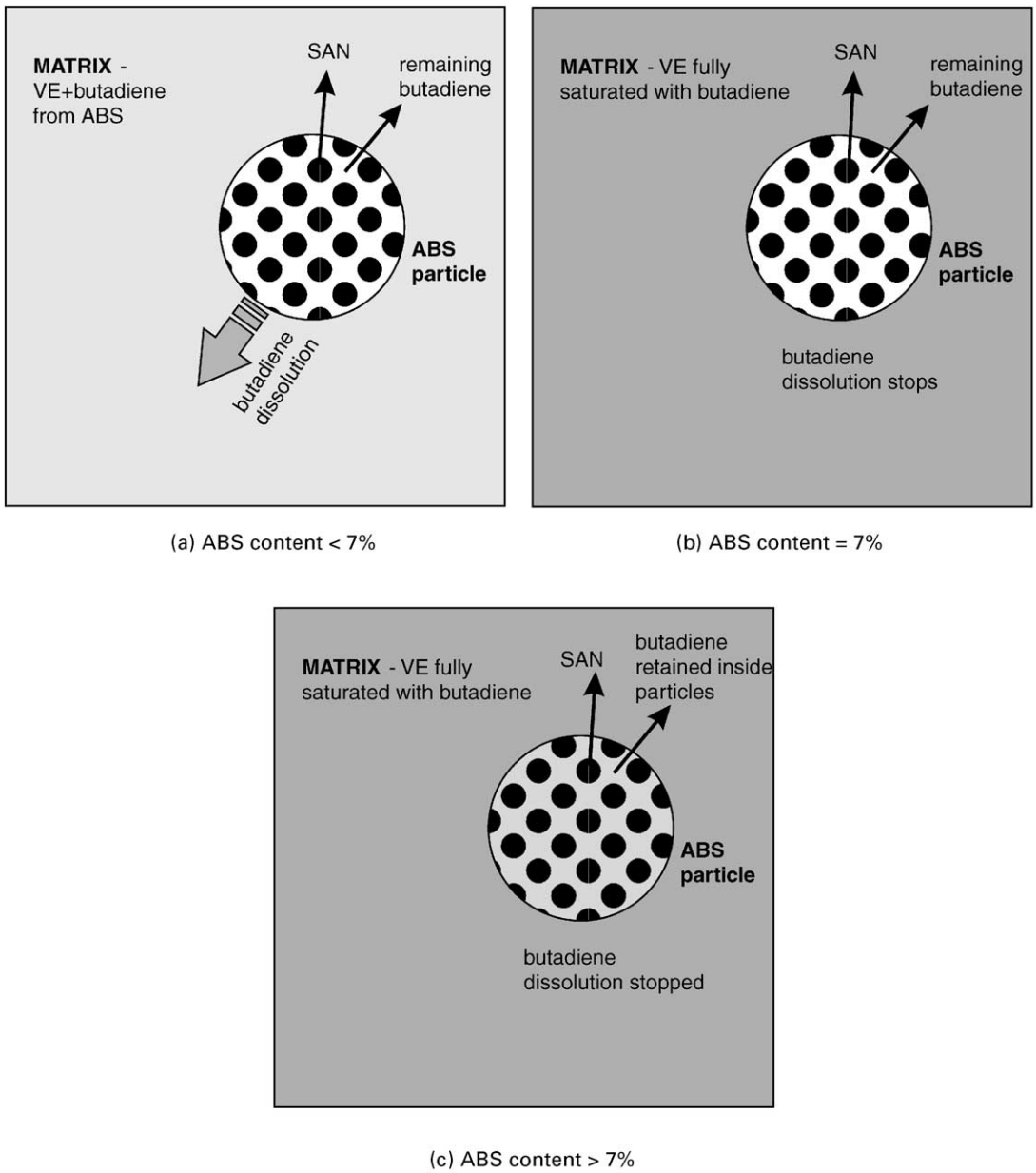

Fig. 11. Schematic representation of the butadiene migration process (single ABS particle only): (a) Below the saturation point, butadiene migrates from the ABS towards the VE, resulting in higher toughness through chemical modification. Small amounts of particles remain almost wholly in the form of SAN. (b) Butadiene saturation is reached. Any further ABS addition will result in the butadiene remains in the particles since the migration has stopped. Particles still do not have any influence on fracture properties—toughness improvement is still through matrix modification. From this point upwards, the matrix will not change its properties. (c) Beyond the butadiene saturation, the matrix possesses properties of the transitional blend (7% ABS/VE) while the particles, with both butadiene and SAN, possess properties of the original ABS. The particles now have significant influence on fracture toughness.

suitable candidates for interlayer-toughening of the VE-based composite materials. The ABS particles were shown to be a cost-effective alternative to more expensive particulate modifiers (various thermoplastics [3,9,11] or newly developed ionomers [13]).

(2) The study established a non-linear trend for mode I fracture toughness versus ABS content. The possible toughening mechanisms can be correlated to the mechanical influence of the second phase in the form of particles but also to the chemical modification of the VE. The presence of ABS particles increased the overall irreversible deformation of the VE, possibly through increasing stresses and strains within the matrix, promoting its yielding and micro-cracking. Also, the Raman spectroscopy showed significant chemical modification of the constituents, which might be a reason for the initial increase in toughness even with low ABS content blends (i.e. 3.5 and 7%).

(3) The Raman spectroscopy revealed good chemical compatibility between the ABS and the chosen VE 8084 due to the existence of butadiene and styrene in both materials.

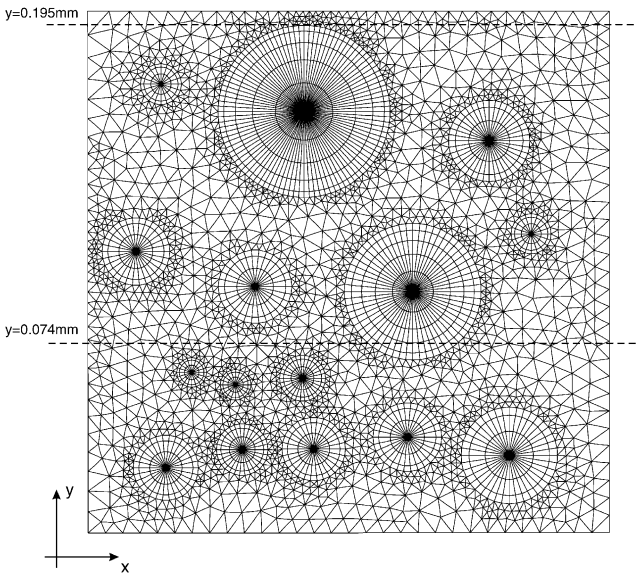

Fig. 12. The final mesh of the tensile model (random particle distribution)—mesh is refined at the matrix/particle interfaces.

Additionally, butadiene migration from ABS particles towards VE was discovered. This process resulted in modified chemical composition of both, VE and ABS. The modification in chemical composition was directly correlated to mechanical properties of the VE/ABS blends. It was assumed that the saturation in the VE modification with butadiene corresponds to change in the fracture toughness trend of the blends, found to be around the level of 7% ABS addition.

(4) By establishing the nature and extent of the chemical modification, a hypothesis regarding the chemical composition of the blends, above and below the butadiene saturation point (7% of ABS), was made. It was assumed that below that level of ABS, the physical presence of the particles does not influence the material's toughness. However, beyond this point, by retaining butadiene, the particles are becoming similar in properties to the initial ABS and start to have a more significant influence on the material's fracture behaviour and toughness. The consequence of this hypothesis is that the 15% ABS/VE blend can be represented by a matrix having the bulk properties of a 7% ABS/VE blend being filled with standard ABS particles. This representation was employed as the input for the finite element analysis of tensile specimens. The aim of the analysis was to show that the model built using the composition hypothesis will produce a stress–strain curve trend similar to that obtained by tensile testing of the 15% ABS/VE blend. The modelling technique achieved this and proved that it can simulate not only a tensile specimen, but can also be applied to a more complex configurations, like interlayer toughened composite laminates.

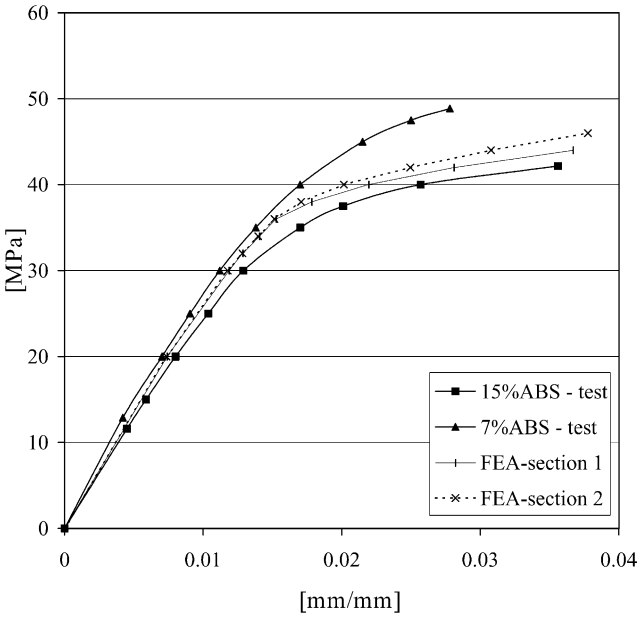

Fig. 13. Experimentally and numerically obtained stress–strain curves—there is a reasonably good agreement between the experimental and numerical stress–strain curves for 15% ABS/VE blend.

Acknowledgments

This research has been supported by the Overseas Postgraduate Research Scholarship (OPRS), ANU PhD Scholarship and TIL (Targeted Institutional Links program). All optical and scanning electron microscope operations were performed with the assistance of the Australian National University Electron Microscopy Unit staff.

References

[1] Chai H. On the correlation between the mode I failure of adhesive joints and laminated composites. Engng Fract Mech 1986;24(3):413–31.
[2] Chai H. Observation of deformation and damage at the tip of cracks in adhesive bonds in shear and assessment of a criterion for fracture. Int J Fract 1993;60:311–26.
[3] Groleau MR, Shi Y-B, Yee AF, Bertram JL, Sue HJ, Yang PC. Mode II fracture of composites interlayered with nylon particles. Compos Sci Technol 1996;56:1223–40.
[4] Ishai O, Sela N. Interlaminar fracture toughness and toughening of laminated composite materials: a review. Composites 1989;20(5):423–35.
[5] Carlsson LA, Aksoy A. Interlaminar shear fracture of interleaved graphite/epoxy composites. Compos Sci Technol 1992;43:55–69.
[6] Singh S, Partridge IK. Mixed-mode fracture in an interleaved carbon-fiber/epoxy composite. Compos Sci Technol 1996;55:319–27.
[7] Chai H. Interlaminar shear fracture of laminated composites. Int J Fract 1990;43:117–31.
[8] Chai H. Micromechanics of shear deformation in cracked bonded joints. Int J Fract 1992;58:223–39.
[9] Sue HJ, Jones RE, Garcia-Meitin EI. Fracture behaviour of model toughened composites under mode I and mode II delaminations. J Mater Sci 1993;28:6381–91.
[10] Woo EM, Mao KL. Evaluation of interlaminar-toughened poly(ether imide)-modified epoxy/carbon fiber composites. Polym Compos 1996;17(6):799–805.

[11] McGrail PT, Jenkins D. Some aspects of interlaminar toughening: reactively terminated thermoplastic particles in thermoset composites. Polymer 1993;34(4):677–83.
[12] Kageyama K, Kimpara I, Ohsawa I, Hojo M, Kobashima S. Mode I and mode II delamination growth of interlayer toughened carbon/epoxy (T800H/3900-2) composite system. In: Martin RH, editor. Composite materials: fatigue and fracture. ASTM STP 1230, Philadelphia: American Society for Testing and Materials; 1995. p. 19–37.
[13] Hojo M, Matsuda S, Ochiai S, Murakami A, Akimoto H. The role of interleaf/base lamina interphase in toughening mechanism of interleaf-toughened CFRP. 12th International Conference on Composite Materials Proceedings, Paris, France, ICCM 12; 1999.
[14] Jang K, Cho W-J, Ha C-S. Influence of processing method on the fracture toughness of thermoplastic-modified carbon-fibre reinforced epoxy composites. Compos Sci Technol 1999;59:995–1001.
[15] Standard test methods for plane-strain fracture toughness and strain energy release rate of plastic materials. ASTM Standard D 5045-91a, Philadelphia: American Society for Testing and Materials; 1991.
[16] Standard test method for tensile properties of plastics (metric). ASTM Standard D 638M-91a. Philadelphia: American Society for Testing and Materials; 1991.
[17] Fredericks PM. Testing Technology; 1996: August–September no. 7.
[18] Ferraro JR, Nakamoto K. Introductory Raman spectroscopy. Boston: Academic Press; 1994.
[19] Young RJ. Key Engng Mater 1996;117:173–92.
[20] Lu Y, Wu F, Xue G, Wang X. Compos Interf 1994;2(4):265–74.
[21] Gu X, Young RJ, Day RJ. J Mater Sci 1995;30:1409–19.
[22] Gu X, Young RJ. Textile Res J 1997;67(2):93–100.
[23] James MA. A plane stress finite element model for elastic–plastic mode I/II crack growth. PhD Thesis. Department of Mechanical and Nuclear Engineering, Kansas State University; 1998.
[24] Jar P-YB. Private communication; 1999.
[25] Kinloch AJ, Young KJ. Fracture behaviour of polymers. Amsterdam: Elsevier; 1983.
[26] Dow Chemicals. Typical room-temperature mechanical properties for Derakane 8084 vinyl ester resin.
[27] Broek D. Elementary engineering fracture mechanics, 4th ed. Dordrecht, The Netherlands: Martinus Nijhoff Publishers; 1986.
[28] Stevanovic D. Delamination properties of a vinyl-ester/glass fibre composite toughened by particulate-modified interlayers. PhD Thesis. Department of Engineering and Information Technology, The Australian National University; September 2001.